CIMAC CONGRESS 25
ZURICH, MAY 19 – 23, 2025

2025 | 281

CFD Simulation of Hydrogen Combustion in an Optical Engine - Focus on Thermodynamic Differences

Simulation Technologies, Digital Twins and Complex System Simulation

Evelyn Flesch, Technical University of Munich (TUM), Institute of Sustainable Mobile Powertrains

Wilhelm Dürrholder, Technical University of Munich, Institute of Sustainable Mobile Powertrains
Maximilian Prager, Technical University of Munich, Institute of Sustainable Mobile Powertrains
Malte Jaensch, Technical University of Munich, Institute of Sustainable Mobile Powertrains

This paper has been presented and published at the 31st CIMAC World Congress 2025 in Zürich, Switzerland. The CIMAC Congress is held every three years, each time in a different member country. The Congress program centres around the presentation of Technical Papers on engine research and development, application engineering on the original equipment side and engine operation and maintenance on the end-user side. The themes of the 2025 event included Digitalization & Connectivity for different applications, System Integration & Hybridization, Electrification & Fuel Cells Development, Emission Reduction Technologies, Conventional and New Fuels, Dual Fuel Engines, Lubricants, Product Development of Gas and Diesel Engines, Components & Tribology, Turbochargers, Controls & Automation, Engine Thermondynamis, Simulation Technologies as well as Basic Research & Advanced Engineering.

ABSTRACT

Man-made climate change necessitates the rapid development of net-zero carbon dioxide emission engine concepts. A promising approach is aimed at the HydroPoLEn Project, namely, to power large-bore engines for marine applications with 100 % hydrogen. However, hydrogen introduces unique challenges compared to conventional gaseous fuels like LNG due to its wide flammability range and short quenching distance. Key combustion phenomena, particularly in close-to-wall regions and crevice volumes, significantly influence the performance of optical engines and must be accurately modelled to ensure reliable results. This study presents a highly accurate 3D-CFD model of the Institute of Sustainable Mobile Powertrains' (NMA) full-scale optical engine. It is developed using Converge CFD software and validated with experimental data.

Optical engines, by design, have larger crevice volumes than comparable thermodynamic engines. Those crevice volumes increase the surface of the compression volume. Additionally, the crevice surfaces that house sealings between different parts of the optical head-liner configuration, are close to cooling mechanisms. Therefore, their thermodynamic characteristic must be modelled accurately. The presented model reproduces the substantial thermodynamic losses in the enlarged crevice volumes of optical engines. In the compression phase, up to 10 % of the gas volume and 20 % of the gaseous mass are contained within crevice volumes. Thereafter thermal losses in those crevice volumes make it necessary to adapt the standard CFD validation process. These enlarged crevice volumes substantially impact the thermodynamic and combustion behavior of the optical engine. Following it makes their accurate representation in simulations critical for understanding hydrogen combustion. The Institute’s optical engine (d 170 mm / 210 mm, 4.8 l displacement) operates in a Bowditch design with full optical access or in a thermodynamic configuration. Optical engines offer wide-range insight into actual combustion behavior, but operating a full optical engine at up to 100 % hydrogen is challenging. With its simulation, a deeper understanding of the specific effects of hydrogen combustion is gained. Those effects of hydrogen are the same in thermodynamic engines, like, for example, the short quenching distance, leading to oil evaporation and combustion within engine loss volumes. Understanding the challenges that arise with hydrogen as a promising alternative fuel is a crucial element in developing new hydrogen combustion processes.

This work describes a validation method for CFD simulation of hydrogen combustion in a full optical large-bore engine, focusing on the thermodynamic differences and heat losses in crevice volumes. Understanding these effects will aid in developing next-generation heavy-duty engines capable of operating on 100 % hydrogen. This is a crucial step toward achieving greenhouse gas neutrality and the main goal of the HydroPoLEn Project.

1 INTRODUCTION

Fully hydrogen-fuelled internal combustion engines (ICE) are an important part of the world's race to decarbonize our future. Hydrogen, which can be efficiently produced using electricity and is entirely carbon-free, offers a viable solution for storing the energy required for remote power applications, such as in the maritime sector. Hydrogen combustion in internal combustion engines is a strongly awaited technology on the way to carbon neutrality. But it still has major challenges to tackle. There are plenty of combustion anomalies like preignition, backfire, knock, and lube oil ignition that come along with the technology of hydrogen ICEs. Therefore, the divergent fuel properties of hydrogen compared to hydrocarbons are not yet completely controllable. To gain more knowledge about the combustion anomalies that arise with hydrogen combustion, optical engines, and CFD simulations are well-established methods to investigate and develop new hydrogen combustion processes. Hydrogen's wide flammability range, its short quenching distance, and its high laminar burning velocity are some of the challenging fuel properties that are shown in Table 1. However, full-scale optical engines give a wide-range insight into actual combustion behavior compared to, for example, optical engines with endoscopes, which only allow a view of specific parts or regions of the engine. Due to the differences in design and operation between optical and classical engines, the standard CFD simulation routine must be adapted for optical engines. The proper modelling of full-scale optical engines in CFD simulation is important to understanding the origin of combustion anomalies and finding new solutions on how they can be avoided. There remain differences between thermodynamic engines and optical engines, and those have to be addressed properly when modelling those optical engines in CFD simulations. For example, optical engines have different sealing mechanisms in the piston-liner area; they don't use oil because this would disturb visibility. In oil-less optical engines, the sealings are made of PTFE or elastomer O-rings, for example. These sealings often have to be set backward to reduce their thermal stress. This method is commonly used in optical engines, but it increases the compression volume [1–3]. This leads to a main combustion chamber similar in shape to the ones in thermodynamic engines but with increased crevice volumes. Based on crevice measurements from CAD, this work describes the effects of those increased crevice volumes on the combustion processes within the optical engine.

Unlike motored operation, where the effect of crevice volumes is insignificant, those crevices gain influence on fired operation, with thermodynamics and heat exchange processes. Usually, the parts that house the sealings are close to internal cooling systems. This means the wall temperatures of those gaps, which increase the cylinder volume, stay cold, a little above the cooling water temperature. Even during combustion, those crevice wall temperatures stay quite low in an optical engine. This is caused by the skip fire mode of optical engines, which typically drive only a few dozen fired cycles in succession to avoid thermal damage to the components.

The wall temperatures of the main combustion chamber behave differently. Due to the high gas temperatures during fired cycles, those main combustion area walls will be hotter. When it comes to hydrogen combustion, this effect is even more substantial because of hydrogens' smaller quenching distance and the higher flame temperature of hydrogen compared to hydrocarbons. With the very high flame speeds of hydrogen and the resulting higher convection of hydrogen, the thermal load on wall components rises above the one caused by hydrocarbons. [4]

Table 1. Comparison of thermodynamic-relevant fuel properties of hydrogen (H_2) and natural gas (CH_4) listed in [5].

Fuel Property	H_2	CH_4
Density	0.08 kg/m³	0.65 kg/m³
Quenching Distance	0.64 mm	2.03 mm
Laminar Burning Velocity	1.85 m/s	0.38 m/s
Adiabatic Flame Temperature	2403 K	2243 K
Minimum Ignition Energy	0.02 mJ	0.28 mJ
Ignitability Range in Air	4 to 75 vol%	5 to 15 vol%

In summary, these physical properties of hydrogen lead to higher wall temperatures during combustion cycles compared to conventional hydrocarbons used in gas ICE [4,6]. When it comes to optical engines that use quartz glass pistons with reduced heat conductivity, these different hydrogen combustion properties seem relevant. Quartz glass has a strongly reduced thermal conductivity compared to metal pistons (1:30 of steel, 1:200 of aluminum). To reduce the thermal stress on the glass, those engines are being run only a few cycles during one load point. As a result, the wall temperatures of the steel housing don't rise much compared to motored cycles. The opposite happens with the glass piston and its reduced thermal conductivity. The glass piston surface gets very hot with the hydrogen combustion characteristics shown in Table 1. CFD simulations are the right tool to determine the influence of those glass-surface temperatures. In a standard CFD approach, the first step is the validation of the load exchange in a cold flow simulation. Then, in the second approach, the wall temperatures are evaluated for the fired cycles. Due to the increased

crevice volumes and their different temperatures and heat transfer characteristics, this approach has to be adapted for optical engines. For the simulation of a fully optical engine, the following points must be taken into account:

- Main combustion area and combustion-relevant crevice volumes must be modelled accurately.
- Smaller crevices volumes of the optical engine that have no relevance to the combustion process must be represented e.g. in a compensation volume.
- The surface temperature of the glass-surfaces facing the main combustion chamber is determined higher at hydrogen combustion. This results from the different combustion characteristics of hydrogen and the reduced thermal conductivity of quartz glass.

The research on optical engines and their modelling in CFD simulations was enabled by the HydroPoLEn Project. The HydoPoLEn Project is funded by the German Federal Ministry for Economic Affairs and Climate Action and aims to develop a large-bore engine for marine applications that runs on 100 percent Hydrogen. Therefore, the project focuses on a better understanding of the combustion processes of Hydrogen, the development of innovative ignition and injection systems, and the optimization of the tribological system that interacts with Hydrogen as an innovative fuel. At the Institute of Sustainable Mobile Powertrains, a single-cylinder test rig with two configurations is used to investigate those combustion anomalies (Figure 1).

The first configuration is the thermodynamic setup, and the second setup has full optical access and is in Bowditch design. The fully optical setup gives detailed insight into ignition and combustion phenomena. To better understand the underlying physical processes, a CFD Simulation model of the optical engine was developed and validated with experimental data. To include all-optical accesses, the liner is split into two parts, and the sealings are recessed. This leads to additional crevices that increase the overall compression volume of the optical engine. To account for this, the CFD validation procedure has to be adapted. A crucial role in the modelling of full-scale optical engines is how to deal with those numerous additional crevice volumes. The presented method replicates the crevices of interest, like the piston top-land and a crevice around the glass of the optical lateral access in detailed geometry. All other crevices are considered by an equivalence simulation compression volume, which is added to the volume of the lateral access crevice.

The optical engine design brings additional load-dependent variations of the compression volume. The volume increases, for example, by the compression of elastic sealings like the elastomer O-rings or the load-dependent reversible deformation of crankshaft bearing gaps, connecting rod, or the Bowditch piston itself.

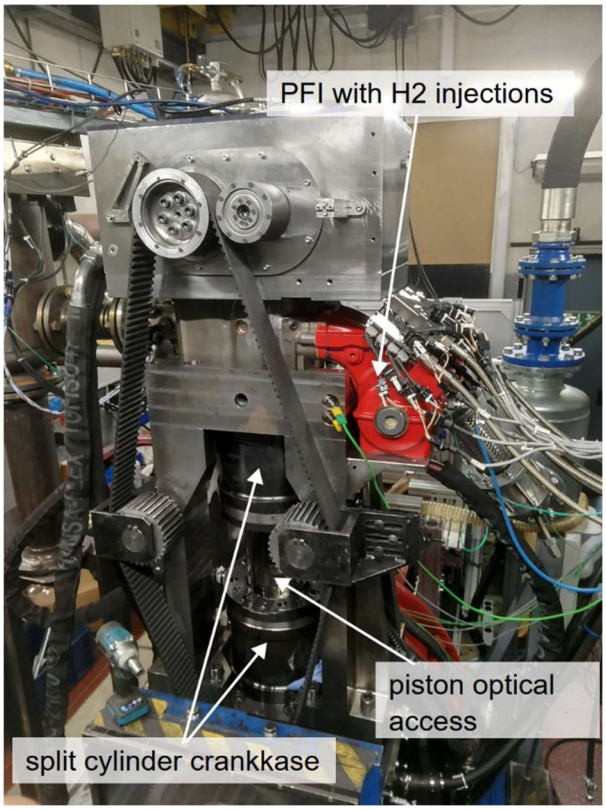

Figure 1. Test Rig of the Institute of Sustainable Mobile Powertrains (NMA) in Bowditch design used to validate the CFD Simulation Model.

In this work a method for setting up a validated CFD model of a full-scale optical engine is presented. This starts with the validation of the compression ratio of an optical engine. It is shown that the dynamic variation of the compression volume has to be considered constant from motored cycles to fired cycles because the deformations at maximum pressure are assumed to be similar.

In a second step the wall temperatures of the optical CFD model are evaluated. It is shown that the influence of the heat transfer within all additional crevice volumes cannot be neglected. Opposite to conventional thermodynamic engine simulations, those crevice wall temperatures are

lower and lead to a higher gaseous mass fraction within those additional crevice volumes.

In a third step the influence of the hot glass-surface temperature in the main combustion chamber is investigated. The reduced thermal conductivity of the optical elements – namely quartz-glass surfaces – leads to a rise in temperature, when interfering with hot combustion gasses. Possible glass surfaces temperatures are investigated and their effect on load exchange and total mass distribution is shown.

In this work a method is proposed to model a full-scale optical engine. Special attention was paid to compression ratio validation and the appropriate choice of dominating wall temperatures. Namely, the temperatures of the quartz-glass surfaces connected to the main combustion chamber are relevant. It can be shown that these hot surfaces influence load exchange, the maximum pressure level, and the total cylinder mass after load exchange. As a consequence, these hot glass surface temperatures and the thermal losses in additional crevice volumes – characteristic for optical engines - have to be determined carefully to model a full optical hydrogen fuelled engine.

2 EXPERIMENTAL SETUP IN BOWDITCH DESIGN

The test rig used for the experimental investigations is a fully optical accessible single-cylinder engine. The engine has a bore of 170 mm and a stroke of 210 mm. Its displacement volume is 4,8 l. Hydrogen is applied via port-fuel injection (PFI) through a two-channelled plenum (Figure 1, Figure 2, Table 2).

Table 2. Engine parameters of the full optical research engine at the Institute of Sustainable Mobile Powertrains at TUM [7].

Parameter	Value
Bore x Stroke	170 mm x 210 mm
Swept Volume	4,77 l
Compression Ratio	Adjustable
Optical Access – piston	Piston Window Ø105 mm Piston Bowl (Ø120 mm) completely visible
Lateral Optical Access - liner	120 mm x 36 mm entire combustion chamber
Peak Pressure	300 bar – by design

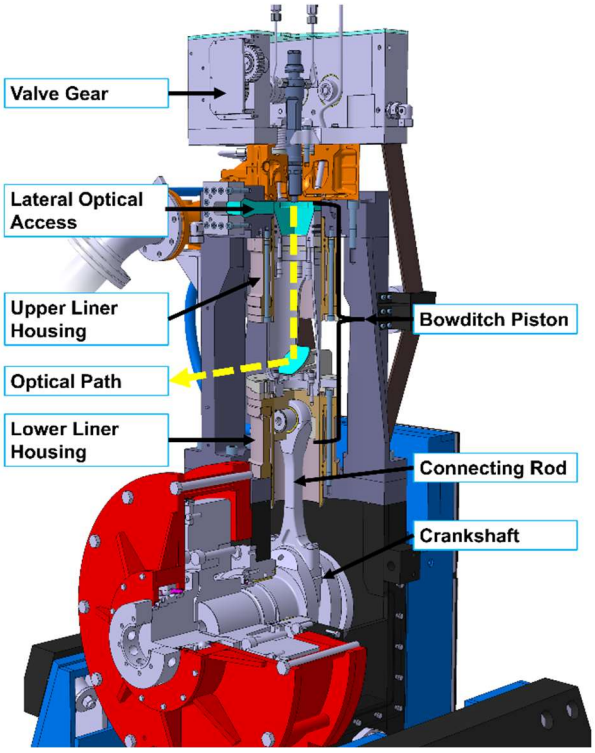

Figure 2. Schematical view of the full optical engine in Bowditch design. The optical path is via a stationary mirror mounted within the split Bowditch piston.

Also varying fuel mixtures with different shares of Hydrogen and Natural Gas can easily be applied through the usage of various magnet valves [8]. The single-cylinder engine is driven with full optical access in Bowditch design [9]. Therefore, an elongated piston with a glass crown of 105 mm of flat vision field is applied. Close to the cylinder head, another glass window allows lateral optical access to the combustion chamber. A schematic view of the test rig and its optical accesses can be seen in Figure 2 and Figure 3. The main optical access is via the glass piston. Whereas the lateral optical access is for supplementary illumination, if needed or to get additional optical data that is close to the intake and exhaust valves. Alternatively, a design with endoscopes can be applied to this section of the engine. This endoscopic setup can also be used with the alternative thermodynamic setup of NMA's single-cylinder engine. Backfire events in hydrogen combustion were investigated with the endoscopic setup of NMA's single-cylinder setup. [10–13]

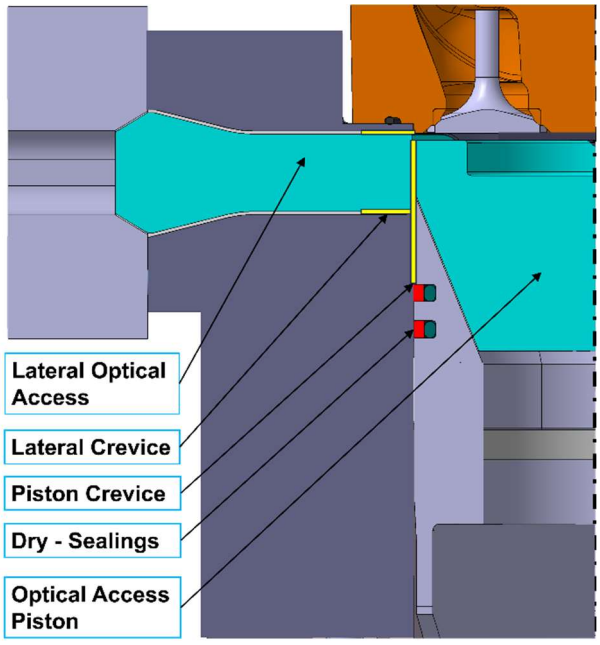

Figure 3. The Optical Accesses are realized with quartz glasses (Cornering 2F). The dry piston rings are made of PTFE (red). The remaining crevices (in yellow) are typical for optical engines.

To evaluate the origin of combustion anomalies, the test program was started with measurements on the fully optical configuration. In the first approach, 100 percent hydrogen was applied. But irregular combustion occurred too frequently. For this reason, a fuel mixture of methane and hydrogen was used, and the proportion of hydrogen was slowly increased. In this way tests with mixtures above 90 % of hydrogen were concluded. The resulting measurement data is the basis of the validation process of the full optical CFD simulation model. The aim is to get a better understanding of irregular combustion through the CFD simulations and to find strategies to develop stable hydrogen combustion processes.

3 CFD SIMULATION MODEL SETUP

3.1 Geometrical Setup of the CFD simulation

The geometry of the optical single-cylinder test engine is derived from CAD data and can be seen in Figure 4. It consists of a plenum that is modelled to the cross-section, where the pressure sensor is mounted. This is the inflow boundary of the CFD model (highlighted red surface, Figure 4). The plenum has two branches that house the port-fuel injection system. In this work, we assumed the inflow boundary to be premixed and did not simulate the PFI mixing processes. Those plenum branches are mounted directly to the cylinder head intake ports (brown surface, Figure 4). The gas path of both exhaust valves is already united within the cylinder head, and the pressure sensor for the outflow pressure trace is mounted at the end of the exhaust port. The piston top-land (purple, Figure 4) is modelled until the first piston ring. The crevice volume of the lateral optical access is shown in blue, and the liner is partially colored in green. The static position of the piston in TDC (Top Dead Center) is measured directly at the test site and applied to the CFD model ($\Delta x = 14{,}4\ mm$).

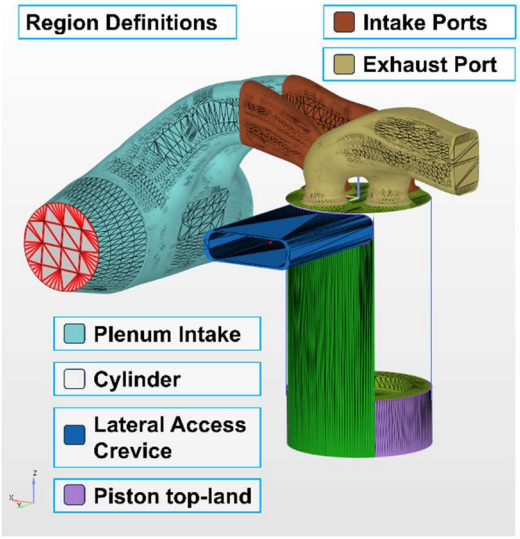

Figure 4. Geometry of full optical CFD simulation model.

The model consists of several regions (enumeration taken from the CFD setup), that describe the following volumes, each with its own characteristics.

- Cylinder Region 0
- Intake Region 1
- Exhaust Region 2
- Piston Crevice Region 4
- Plenum Intake Region 5
- Lateral Access Crevice Region 7

All surfaces represent the original CAD Design of the single-cylinder test engine, including the piston top-land. This geometric exact modeling is necessary to show the flame propagation into the piston top-land to get information on how deep the flame burns into this crevice or whether unburnt hydrogen remains in the crevice. However, optical engines have, by design, a large amount of crevice regions. To model all those with full geometric accuracy would cause immense computational costs. But still, those crevice volumes influence the

engine behavior strongly. Especially when it comes to load exchange, they are not neglectable anymore. All additional crevice volumes were measured as exactly as possible in CAD. When it comes to compressible sealings, the shape was adapted to a deformed state under pressure load. Figure 5 gives an impression of all those additional crevice volumes.

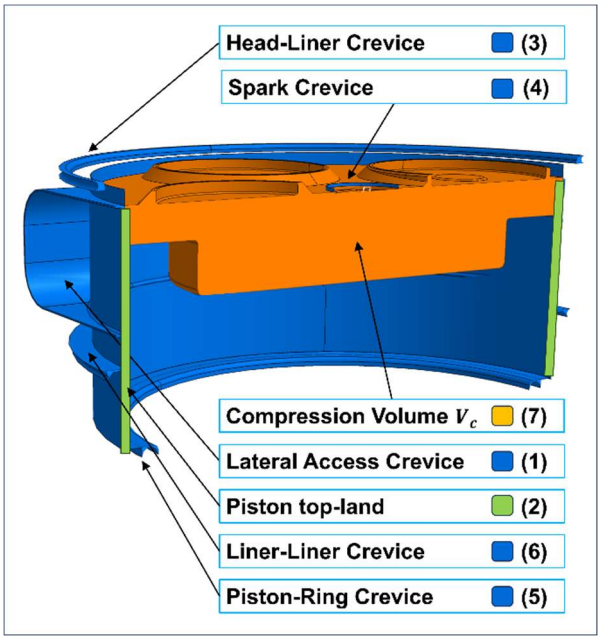

Figure 5. Overview of all crevice volumes of the optical engine that enlarge the compression volume.

3.2 Numerical Setup of the CFD simulation

The simulation for this single-cylinder full optical engine was set up with the commercial software Converge, version 3.19 [14]. Reynolds-averaged Navier Stokes equations were applied to solve the fluid partial equations, and the turbulence model k-ε was utilized. The Converge software includes an Adaptive Mesh Refinement (AMR), which automatically refines the grid based on fluctuating and moving conditions such as temperature or velocity. In this work, the sub-grid scale (sgs) based AMR with different scales is applied (Table 3). A base grid size (bgs) of 12 mm was chosen for the whole simulation volume. The grid generation is made by the Converge solver in runtime. When it comes to cut cells, Converge uses cell-pairing when the volume of the cut cell is smaller than 1/3 of the base grid cell. In the thin crevice volumes of piston top-land and lateral access crevice this happened frequently. Therefore, a fixed embedding was applied that scales those crevice cells down to a reasonable amount. In this way, the fluid quantities are solved properly, and the calculation time is still acceptable. Table 3 gives an overview of the applied mesh refinements. The resulting grid-size (gs_{res}) for each physical quantity is calculated via

$$gs_{res} = \frac{bgs}{2^{Scale}}$$

Combustion was modelled using the GRI3.0 reaction mechanism. This mechanism fits well with hydrogen and includes hydrocarbons as well. For pure hydrogen combustion simulations, the Converge hydrogen mechanism (Conv3.0) shows the best results (CIMAC 2025, Paper No. 045). But for simulating the described experimental setup, the CH_4 mechanisms will have to be added to Conv3.0 first. [15–17]

Table 3. Meshing strategy of the full optical CFD simulation model.

Mesh Parameter	Value	Application
Base Grid Size	12 mm	
Temperature AMR	Scale 5 (SGS 2,5)	Region 0 (Cylinder) Permanent
	Scale 5 (SGS 2,5)	Region 4, 7 (Crevice Regions) 705 – 190 CAD During combustion
Velocity AMR	Scale 3 (SGS 10)	Region 0, 1 (Cylinder, Intake) Permanent
Boundary Embeddings	Scale 2 – 4	Plenty
Region Embeddings	Scale 4	Region 4, 7 (Crevice Regions)
	Scale 1	Region 1, 5 (Intake, Plenum)
Shape Embeddings	Scale 2	Cylinder Shape Including combustion chamber and valves
	Scale 4 - 6	Sphere Shape Around source

3.3 Measurement Data Handling for Simulation Validation

Indicated data was recorded at 0.1 CAD resolution, while slow data was recorded and averaged over one working cycle. As inputs for the performed simulations, the gas parameters are used. This is, namely, the indicated pressure profile of plenum pressure and exhaust pressure. The temperatures are measured at the same locations and consist of one, quasi-static value per working point. At the plenum, the inflow temperature was 310 K, and at the exhaust, the outflow temperature was 667 K. Ignition is at 713,5 CAD, and the gas composition at plenum inflow is assumed to be premixed with an air-fuel equivalence ratio (AFER) of 2. For validation, the indicated pressure profile of the incylinder pressure measurement is used.

4 RESULTS

4.1 Compression Ratio Validation

For compression ratio validation, two motored operating points were used, one before and one after the optical tests. The engine was conditioned properly, so it is assumed that the wall temperatures are uniform at the level of cooling water temperature, which is 370 K. The compression ratio is evaluated with the first operating point and checked with the last operating point, because after all fired working cycles differences in wall temperatures are possible.

In this CFD model, the piston top-land is modelled exactly until the beginning of the first piston ring groove. The PTFE sealings have an elastomer O-ring within the groove, that guarantees the tight seat of the sealing within the groove. The volume within the groove depends on the compressed shape of the O-ring and is not added to the piston top-land volume. But it is accounted for in an additional compensation volume.

There are several other smaller crevices in this optical engine geometry. These result from sealings set backward to withstand high temperatures and those are often realized by elastomer O-rings. Those sealing volumes have in common, that their absolute volume is changing, depending on the motion and pressure profile of the operating points of the optical engine.

During the validation process, it was obvious that those crevice volumes have a great impact on the compression ratio. In cold flow, where all wall temperatures are assumed to be equal, the impact is not that high. But with fired cycles, the wall temperatures within the main combustion chamber rise significantly over the ones within the crevice volumes. Those crevice volume wall temperatures are dominated by the cooling circuits of the engine. Therefore, their temperatures are assumed to stay close to the wall temperatures in cold flow simulation.

In this simulation model, not every single volume change should be modelled properly; the aim is to get a good impression of the processes in the main combustion chamber. Therefore, the simulation volume is divided into three different regions (enumerated as in CFD setup).

- **Main Cylinder Region (0)** is the cylinder volume without crevices and is dominated by loading and combustion processes
- **Piston Top-Land Region (4)** gives a geometric exact reproduction of the piston crevice and can reproduce the penetrating flame and the combustion processes within the piston top-land.
- **Compensation Region (7)** is realized as prolonged lateral access. Because it is the biggest crevice within the optical engine.

By designing the compensation volume as lateral access, the aim was to reproduce the physical properties of all crevice volumes. Therefore, the lateral access crevice wasn't only prolonged because this would lead to long combustion processes while the flame wanders deeper into the crevice. To enlarge the compensation volume the crevice was first prolonged and then made broader at the rear side. This was repeated a few times until the aimed compression ratio was reached. This procedure should ensure that the connection surface to the main combustion chamber is still accurately reproduced. In Figure 5, it can be seen that the surfaces that connect the additional volumes to the main combustion chamber are neglectable. But the attached volumes of those crevices (3,4,5, and 6) are of relevance for the further procedure. The compensation volume should account for those various crevice volumes shown in Figure 5. The design of the compensation volume as lateral access followed the principle that it reproduces the volume of those additional crevices and aims at reproducing the heat exchange characteristics of those wall-temperature-dominated crevice regions. The heat exchange characteristics are a function of variant parameters (e.g. volume-to-surface ratio, turbulence, surface roughness) and it would be numerically too expensive to model them in full scale. Therefore a numerical possible model compensation volume was created. For example, a very long lateral access with a constant surface area as compensation volume wouldn't account for the plenty of small crevice volumes of the engine. Because the gas exchange wouldn't be the same.

The crevice volumes are wall-temperature-dominated regions. Because their surface to fluid volume is high compared to the main combustion chamber. Because they are more a sum of small volumes than one big volume, their gas and pressure equalization happens faster than the one of a prolonged crevice. Therefore, the crevice volume of the model was added in a good trade-off of all parameters. This means that the entry to lateral access was kept constant (represents all small entries of the crevices), but backward, the crevice was made step by step broader and longer. This ensures a good turbulence level to get good heat exchange with the cooler crevice wall temperatures, but it also allows a backward exchange of the crevice gasses with the main combustion chamber. If the crevice were long and thin, this exchange with the main combustion

chamber couldn't be accounted for. Table 4 shows an overview of the varied parameters of the prolonged lateral access to compensate for the crevice volumes of the optical engine.

Table 4. The geometrical design of the compensation volume is realized as the expansion in depth and width of the lateral access crevice.

Compression ratio (CR) (constant TDC position)	Depth of lateral access (m)	Surface-to-volume ratio of compensation volume
9,7	0.100	5.15
9,4	0.100	5.13
9,2	0.100	5.10
8,9	0.150	7.34
8,7	0.150	7.27

The piston position at TDC (14.4 mm, between piston crown and head) was measured at the test site and adapted for the CFD simulation. With all crevice volumes measured out of CAD data, a compression ratio of 9.2 was calculated. This is referred to as static compression ratio ε_{stat}.

$$\varepsilon_{stat} = 9.2$$

When the simulated cylinder pressure was compared to the motored measurement data, the compression volume under load was found to be larger than the static volume gained from CAD data. This is caused by the sealing deformations under compression. This compression ratio under load is further referred to as dynamic compression ratio ε_{dyn}. The best result of the dynamic compression ratio of all cold flow simulations listed in Table 4 was a value of 8.7 for the dynamic compression ratio. The deviation at peak pressure is +0.8 %.

$$\varepsilon_{dyn} = 8.7$$

Figure 6 shows the different cylinder pressure traces compared to the measurement data point.

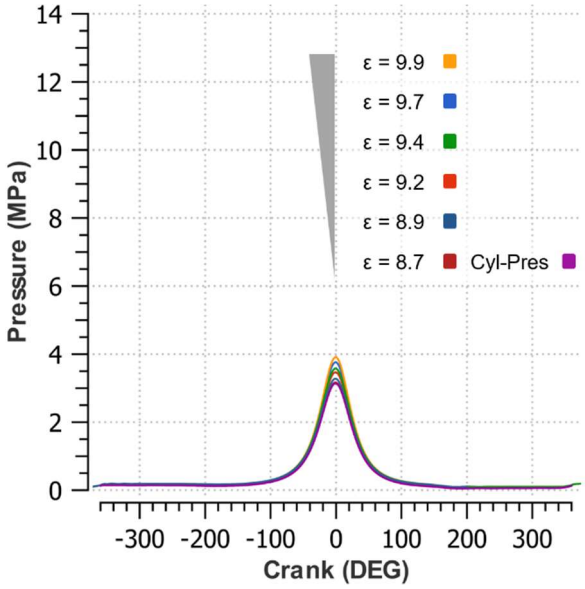

Figure 6. Variation of the compensation volume to validate the compression ratio with a motored operating point.

4.2 Wall-Temperature Modell of Fired Cycles

The next step in the standard CFD routine is to determine and validate the wall temperatures of the fired operating points. In standard thermodynamic engines, one operating point is driven for a long time so that the wall temperatures get constant at this operating point. When the wall temperatures are constant, a wall temperature model can be derived in CFD simulation by comparing the cylinder pressure traces.

At a full-scale optical engine, the operating mode is different. Because of the reduced thermal resistance of the quartz-glass piston, there are only a few dozen fired cycles possible in a row. Those fired cycles are followed by motored cycles to cool down the engine. At the test site, self-ignition was experienced even in motored cycles when the engine was motored with hydrogen and methane. To avoid damage to the glass parts, the following operation scheme was designed for each operating point

- motor with ignition
- gas application & fired cycles
- motor with ignition and turn off the gas application

With this scheme, about 70 fired cycles were measured for each operating point, surrounded by the motored cycles. The motored cycles before firing are called motored pre and the motored cycles after the fired ones are called motored post.

To validate the wall temperatures, we initially aimed to determine the average wall temperatures over the whole measurement. In the first approach, the mean pressure value was calculated across all cycles, including both motored-pre, motored-post, and fired ones. However, this method proved ineffective. Subsequently, we calculated the mean pressure based solely on all motored cycles, but this approach also remained imprecise.

A more refined method was then implemented. This involves the use of six motored cycles prior to ignition (motored-pre) and six motored cycles following ignition (motored-post). This approach appeared promising for estimating the average wall temperatures of the fired cycles. It was assumed that pre-motored cycles represent cold wall conditions, while post-motored cycles represent the highest wall temperatures of the fired cycles. Between these two phases, wall temperatures were assumed to increase from pre-motored to post-motored levels.

However, this assumption failed to align with the observed cylinder pressure curves. To address this discrepancy, the experimental pressure data was analyzed in greater detail.

4.3 Experimental Data Findings

Figure 7 shows a qualitative overview of the cylinder pressure of all 150 cycles within one operating point. A wide cycle-to-cycle variation of the pressure curves can be found. First, there are the motored pressure curves, showing a variation in the maximum pressure level. Second, the fired cycles vary even stronger in the maximum pressure. The shape of the combustion curve, however, is almost constant, and the ignition time is constant as well. Last, there are motored cycles after the fired ones, which again show a variation in the maximum compression pressure. There is one intermediate cycle (Figure 7, purple line) that shows a wider pressure peak. Although the cycle is not fired anymore. The assumption that the pressure of the fired cycles rises constantly from every single cycle to cycle couldn't be found. But when averaged over 10-20 cycles this tendency of rising peak pressure with proceeding operation time could be observed.

In summary, a dependency of cylinder pressure on motor operation time can be found. The later the fired cycles, the higher the peak cylinder pressure of those averaged cycles is.

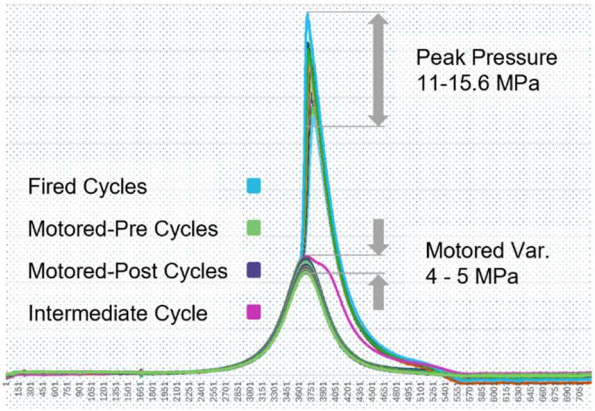

Figure 7. Qualitative cylinder pressure cycle variation within one working point.

In a more detailed examination of the load exchange phase, two distinct shapes of pressure profiles can also be identified (Figure 8). At load exchange the motored-pre (blue) and motored-post (red) cylinder pressures are similar. But at fired cycles, the cylinder pressure curve (green) shows a completely different behavior. Its level is much lower than the ones of motored cycles and it shows an increasing cylinder pressure during load exchange. When the intake valve closes, the cylinder pressure hasn't reached the pressure level of intake pressure. But usually, pressure equivalence of intake pressure and cylinder pressure is assumed at the intake valve closing during the intake valve open (IVO) phase. This is relevant to get a proper load exchange of the engine.

When plotting different average pressure values of the fired cycles, it could be shown that the later the cycles were, the lower the pressure level gets during IVO. The later the cycles, the hotter the wall temperatures, is another unwritten statement when running an optical engine with glass surfaces.

The expectation was that the pressure curve of the fired cycles should lie in between the motored-pre and motored-post pressures. Therefore, a median wall temperature model was evaluated, assuming that the wall temperatures are hot after the fired cycles and cold before the fired cycles.

The deviation between motored and fired pressure curves during the load exchange phase is critical for determining the total cylinder gas mass after load exchange. If the pressure levels have not equalized between the intake region and the cylinder region at the end of the intake valve opening (IVO) phase, it indicates that the load exchange process hasn't been fully completed at that point in time.

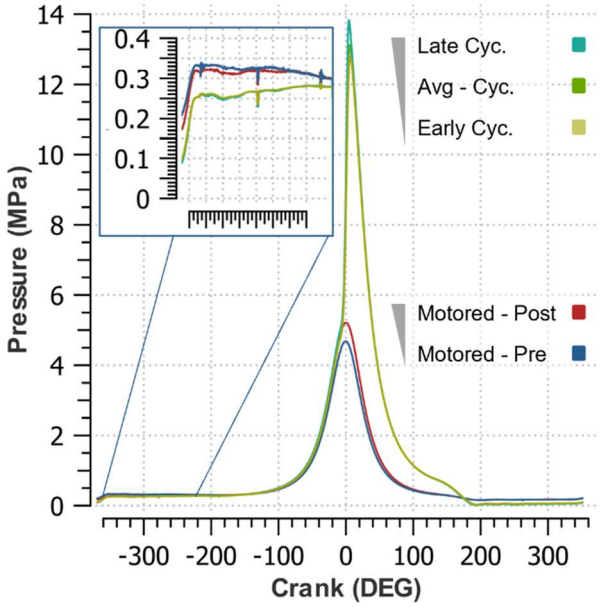

Figure 8. Cylinder Pressure traces during a fired working point. During the load exchange phase, the characteristic of fired cycles differs significantly.

The observed pressure differences during load exchange suggest the presence of a significant factor differentiating motored cycles from fired cycles. The most apparent influence is the combustion process during fired cycles. Combustion leads to a rapid increase in cylinder pressure and a sharp rise in the combustion chamber temperature. The hydrogen flame burns closer to the walls due to its shorter quenching distance, which results in increased wall temperatures. At surfaces with low thermal conductivity, such as glass, the combustion phenomena lead to substantially higher wall temperatures. In the optical-accessible single-cylinder engine used in this study, the surfaces experiencing these higher temperatures are the glass piston surface and the glass liner surface of the lateral optical access. Because both are in direct contact with the main combustion chamber gases.

4.4 Influence of Glass-Surface Temperatures

To evaluate the influence of the glass-surface temperature, a variation with the presented CFD simulation model was conducted. The glass-surface temperatures varied from 670 K, which is the surface temperature determined with methane and diesel pilot ignition [18] up to 1200 K. The other wall temperatures, determined by the cooling mechanisms, are not varied further within this simulation model. Furthermore, the lateral crevice temperature was chosen to be equivalent to the piston top-land temperature. An overview of the chosen temperatures and of the simulated variations of interest is given in Table 5.

Table 5. Wall-Temperature model of the CFD simulations and the variations of glass-surface temperatures that are facing the main combustion chamber.

Surface	Temperature in K	Variation
Liner (metall)	350 K	Const.
Inner Crevices	350 K	Const.
Head	390 K	Const.
Valve Bottom	390 K	Const.
Glass-Piston & Glass-Liner	640 K (V5), 840 K (V6), 1200 K (V7)	Varied

The result of the glass-surface temperature variation on cylinder pressure is shown in Figure 9. The higher the glass-surface temperature is, the higher the maximum combustion pressure gets.

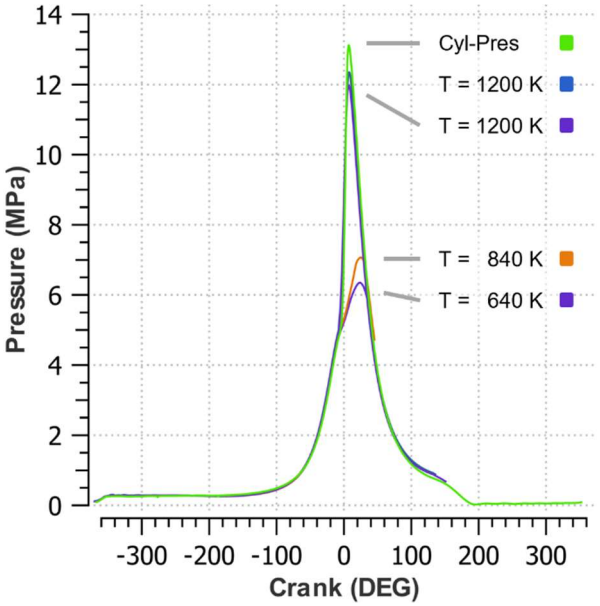

Figure 9. Cylinder pressure at a variation of glass surface temperatures that face the main combustion chamber.

The total mass passing from the intake region to the cylinder region for the same simulations is shown in Figure 10. For 640 K and 840 K glass-surface temperatures, the cylinder mass is almost equal. But when it gets to higher glass-surface temperatures, this has a reducing effect on the total cylinder mass.

The hot glass surfaces seem to heat the entering gas during IVO phase already. The gas expands due to the heating, and following, less gaseous mass can enter the cylinder. The finding that the cylinder mass gets larger when the plenum is added to the intake volume supports this assumption. With the plenum-intake region, the expanding gas finds a larger volume to expand to, and therefore, the loss of in-cylinder density is smaller. Figure 10 shows the integration of the

plenum intake and the effect on cylinder mass in a subsequent cycle.

Consequently, this means that the high glass-surface temperatures have a direct influence on the maximum cylinder pressure. This results from their influence on the early phase of a working cycle, namely the load exchange phase.

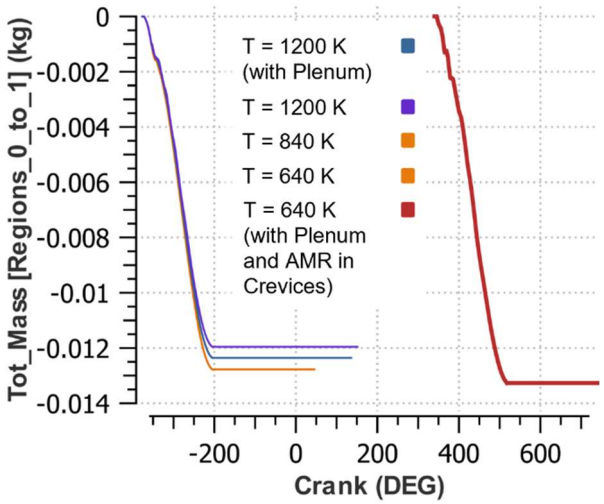

Figure 10. The first cycle (-360 to 175 CAD) shows the total cylinder mass with varying glass-surface temperatures. For the second cycle (360 to 720 CAD), the plenum was added, and the expansion volume increased.

The activation of temperature and velocity AMR not only in the main combustion chamber but especially within the crevice volumes is numerically expensive but crucial to reproducing the thermodynamic characteristics of a full-scale optical engine correctly. By activating the temperature and velocity AMR, the thermodynamically relevant heat losses in the additional crevice volumes of the optical engine can be adequately considered.

When crevice AMR is not activated, as shown in the simulations of the first cycle (from -360 CAD to 200 CAD, Figure 10), the hot glass surfaces heat the entering gas through load exchange. The heated gas expands, and less mass can enter the cylinder when the glass surface temperatures get higher. The cooler crevice wall temperatures cool down the already heated entering loading. This allows up to 20 % of the loaded mass to be stored within those crevice volumes (Table 6). This effect was first demonstrated in a 0D engine simulation with a two-zone model [19,20] and is reproduced and investigated in detail in the presented full-scale optical engine CFD simulation model.

Table 6. Mass distribution at TDC at a motored simulation with activated crevice heat transfer (temperature and velocity AMR).

	Mass at TDC in kg
Cylinder	0.0104243
Piston Top-Land	0.0004521
Compensation Volume	0.0022576
Total Loaded Mass	0.0131340
Sum of Crevice Mass	0.0027097
Proportion of Crevice to Total Mass	20 %

In Figure 11 the distribution of cylinder mass during a motored cycle is shown. Following within the crevices, cooler gaseous mass is stored, and this allows the optical engine to load more cylinder mass, although the gas is heated by the hot glass surfaces at the same time.

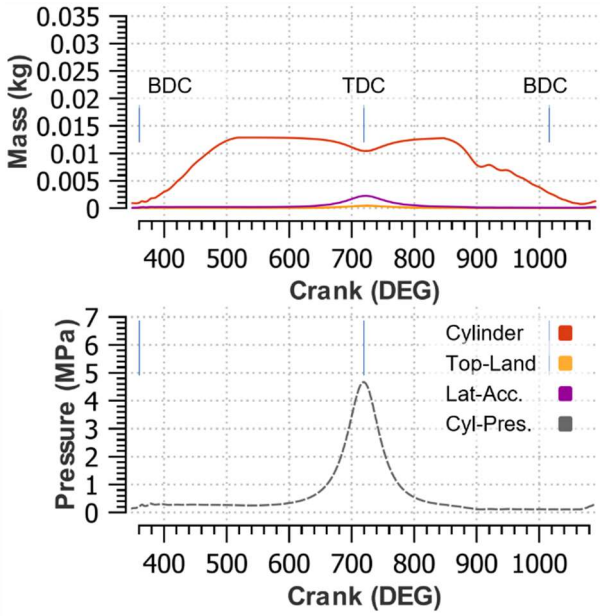

Figure 11. Gaseous mass separation in an optical engine as determined in the developed CFD simulation model.

When temperature AMR is activated in the crevices, like in the second cycle shown in Figure 10, the heat transfer within those crevice volumes is reproduced in the CFD simulation. During a fired simulation this effect might get even stronger. The pressure rise during the working phase of the engine will force additional loading into those crevice volumes. When combustion ends in the main combustion chamber, there are ongoing combustion processes close to the crevice volumes (Figure 12). This observation can explain the widened pressure curve of the cylinder pressure measurements around 70 CAD (Figure 8), which

could be reproduced with the presented CFD simulation model of NMA's full optical engine.

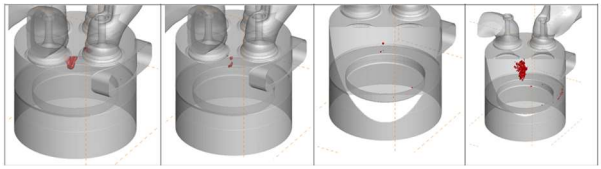

Figure 12. Flame front of hydrogen methane combustion at 2000 K, restarting around 70 CAD.

In this chapter, it could be shown and theoretically explained that the glass-surface temperature does not only have an impact on the maximum compression pressure but also has an impact on the mass flows during load exchange.

5 CONCLUSION OF THERMODYNAMICS DURING LOAD-EXCHANGE

This paper presents a method for developing a validated CFD model of a full-scale optical engine. It confirms that compression volume differs between a theoretical static value and a validated dynamic value due to variations within the sealing volumes that are assumed constant at maximum pressure. Those crevices – typical for all optical engines - are close to cooling mechanisms. Therefore, it could be shown that those crevices are wall-temperature dominated. Consequently, gaseous mass fractions up to 20 % are achieved within the crevices. Within the main cylinder, it could be shown that the combination of hydrogen combustion and quartz-glass surfaces with reduced thermal conductivity led to a strong rise in surface temperatures. Surface temperatures of the glass-piston and lateral access were varied up to 1200 K and their reducing influence on loading and enhancing influence on peak pressure could be shown.

5.1 Influence of glass surface temperature on load exchange

During the load exchange process, air and fuel are introduced into the combustion chamber and its crevice regions. The crevice regions are strongly wall-temperature dominated. Because those crevice materials are close to cooling mechanisms, the gas that enters the crevice regions cools down, and its volume is reduced. This reduction in volume leads to a higher mass concentration within the crevice volumes as shown in Figure 10. The sum of gaseous mass is constant after load exchange, but there is a shift of mass from the cylinder region to crevice regions after the top dead center.

High glass-surface temperatures in the main combustion chamber reduce the mass during load exchange. However, it still leads to higher compression pressures at the same operating point because the trapped gas mass is experiencing further expansion. However, in the presented CFD simulations, the heat transfer within the crevice volumes is modelled, and thereafter, more gas mass can enter during load exchange.

5.2 Thermodynamic Loss Angle

The effect of cooler crevice volumes on the gas phase is shown by measurements of the thermodynamic loss angle on the same single-cylinder engine with a different cylinder head configuration. The piston position around TDC was measured and compared to the cylinder pressure. For the utilized engine parameters on the test bench could be found that the maximum pressure is reached at 1.15 to 1.30 CAD before TDC [19]. This is usually referred to as thermodynamic loss angle. Standard thermodynamic engines usually have a loss angle of 0.5 to 1.0 CAD [21,22]. For the NMA's single-cylinder optical engine, a thermodynamic loss angle of 1.2 CAD was determined on the same optical engine configuration. The mass distribution of the developed CFD simulation model and the mass distributions in cylinder and crevice regions is shown in Figure 11. This reproduces the characteristic of the full-scale optical engine that was measured before at the test site within the developed CFD model. Hence the thermodynamic differences of the optical engine can be reproduced through

- Determining the dynamic compression ratio as described in 4.1
- Modelling a compensation volume, that represents the dynamic compression ratio, as shown in 3.1
- Achieving the optimal glass-surface temperature at the operating point as described in 4.4.

5.3 Materials of Optical Engines

The coupling of a material with reduced thermal conductivity and a fuel that quickly reaches high combustion temperatures and burns close to the walls, like hydrogen does, was estimated to be critical. While validating the CFD simulation to the optical measurement data, it became obvious that this topic had to be addressed within the simulation model. This was the basis for the investigation of the influence of glass-surface temperatures on combustion and load exchange processes.

Standard pistons of thermodynamic engines are made of steel with a high heat transfer coefficient. Cooling is ensured by the good heat flow characteristics of the piston and oil lubrication. An

optical engine is operated without oil lubrication and, therefore, without cooling. This enlarges the impact of fast-rising temperatures, through hydrogen combustion on the glass-surface temperature development. In Table 7 the thermal conductivity of standard piston materials is summarized. The optical piston used in this experimental setup was made of quartz glass of the type Cornering 2F. Sapphire glass would have a higher thermal conductivity, but still the oil-less operation of the engine would lead to high glass-surface temperatures.

Table 7. Thermal conductivity of different standard piston and optical piston materials.

Piston Material	Thermal conductivity
Aluminum	237 W/(mK)
Steel	46 to 50 W/(mK)
Saphir Glass (Schott)	27 W/(mK)
Quartz Glass (Cornering 2F)	1,38 W/(mK)

In section 4.3, Experimental Data Findings, the effect of the hot glass-surface temperatures on the cylinder pressure curves could be shown. The data also shows a time dependency. The effect of the hot surface temperature lasts only for one more cycle, after the fired cycles. After this intermediate state, the mean pressure curve of the motored-post cycles has almost the same shape as the motored-pre cycles (Figure 8). In conclusion, this means the glass-surface temperatures of the glasses facing the main combustion chamber change within one working cycle.

5.4 The next steps in refining this model will be

1. Simulation and validation of the thermodynamic engine setup to get the cylinder head geometry validated
2. Modelling of the hydrogen injection (PFI) to determine the effects of hydrogen stratification
3. Adapting the validated cylinder head model to the full-optical engine model and determining the optimal glass-surface temperatures.
4. Modelling the time dependence of the glass-surface temperature to check whether the assumption of constant glass-surface temperatures over the whole simulation time is appropriate.

Especially hydrogen stratification seems to be of significant relevance as is indicated by experiments (CIMAC 2025, Paper No. 060). and has to be investigated by including the PFI into further simulation models.

Further, within the following simulations, the predicted time dependence of glass-surface temperatures can be reproduced by using a user-defined function in the first approach. Even better would be to apply a 1D - CHT simulation for those glass surfaces of interest. This, in combination with the super-cycling algorithm of Converge, makes it possible to predict the development of the glass surface temperatures over several cycles. In conclusion, an explanation for the observed cycle to cycle variations in cylinder pressure can be given, providing a deeper understanding of the potential of full-scale optical engines as a valuable tool for advancing research on hydrogen combustion.

The CFD model of NMA’s full-scale optical engine provides critical insights into the complex dynamics of hydrogen combustion. While hydrogen's unique physical properties pose challenges in internal combustion engine applications, they also underscore its potential as a transformative alternative fuel. In thermodynamic engines, advancements in stationary operation and robust cooling mechanisms help manage moderate wall temperature rises. Nevertheless, shared concerns between thermodynamic and optical engines - such as hydrogen flames burning closer to walls, crevice volume penetration, and resulting oil evaporation or particle emission changes [23] - highlight areas of ongoing investigation. These challenges, though significant, are met with a concerted research effort, bringing promising solutions within reach and paving the way for hydrogen's sustainable integration into future engine designs.

6 FUNDING

The investigations on optical engines, CFD-simulations, and approaching new hydrogen combustion concepts were part of the HydroPoLEn project, funded by the German Federal Ministry for Economic Affairs and Climate Action based on a decision by the German Bundestag (project no. 03SX570B), which is gratefully acknowledged.

7 ACKNOWLEDGMENTS

Convergent Science provided CONVERGE licenses and technical support for this work. The authors would also like to thank for the prosperous cooperation within the HydroPoLEn project, especially in CFD exchange with our partners MAN Energy Solutions SE and Tenneco.

8 REFERENCES

1. Karmann, S.; Eicheldinger, S.; Prager, M.; Jaensch, M.; Wachtmeister, G. Experimental comparison between an optical and an all-metal large bore engine. *International Journal of Engine Research* **2023**, *24*, 1223–1238, doi:10.1177/14680874221082794.
2. Irimescu, A.; Di Iorio, S.; Merola, S.S.; Sementa, P.; Vaglieco, B.M. Evaluation of compression ratio and blow-by rates for spark ignition engines based on in-cylinder pressure trace analysis. *Energy Conversion and Management* **2018**, *162*, 98–108, doi:10.1016/j.enconman.2018.02.014.
3. Renzis, E. de; Mariani, V.; Bianchi, G.M.; Cazzoli, G.; Falfari, S.; Antetomaso, C.; Irimescu, A. Implementation of a Multi-Zone Numerical Blow-by Model and Its Integration with CFD Simulations for Estimating Collateral Mass and Heat Fluxes in Optical Engines. *Energies* **2021**, *14*, 8566, doi:10.3390/en14248566.
4. Verhelst, S.; Wallner, T. Hydrogen-fueled internal combustion engines. *Progress in Energy and Combustion Science* **2009**, *35*, 490–527, doi:10.1016/j.pecs.2009.08.001.
5. Armbruster, F.; Kraus, C.; Prager, M.; Härtl, M.; Jaensch, M. Optimized Emission Analysis in Hydrogen Internal Combustion Engines: Fourier Transform Infrared Spectroscopy Innovations and Exhaust Humidity Analysis. *SAE Int. J. Engines* **2024**, *17*, doi:10.4271/03-17-07-0052.
6. Flesch, E.; Glocker, E.; Prager, M.; Jaensch, M. Hydrogen Combustion in ICE, Simulation of Optical Engines, Blow-By and Thermal Losses. *Preprints.org MDPI* **2024**, doi:10.20944/preprints202410.0210.v2.
7. Gleis, S. Optische Untersuchung eines diffusiven Dual-Fuel Brennverfahrens für Erdgas sowie alternative Kraftstoffe mit niedriger Zündwilligkeit. Dissertation; Technische Universität München, München, 2023.
8. Eicheldinger, S.; Waligorski, D.; Wachtmeister, G.; Jaensch, M. Performance Potential of Hydrogen Combustion Engines for Industrial Applications. *MTZ Worldw* **2022**, *83*, 60–64, doi:10.1007/s38313-022-0830-8.
9. Bowditch, F.W. A New Tool for Combustion Research A Quartz Piston Engine. In *SAE Technical Paper Series.* Pre-1964 SAE Technical Papers, JAN. 01, 1906; SAE International400 Commonwealth Drive, Warrendale, PA, United States, 1906.
10. Gleis, S. Optische Untersuchung eines diffusiven Dual-Fuel Brennverfahrens für Erdgas sowie alternative Kraftstoffe mit niedriger Zündwilligkeit. Dissertation; Technische Universität München, München, 2023.
11. Karmann, S.; Eicheldinger, S.; Prager, M.; Jaensch, M.; Wachtmeister, G. Optical and Thermodynamic Investigations of a Methane- and Hydrogen-Blend-Fueled Large-Bore Engine Using a Fisheye Optical System. *Energies* **2023**, *16*, 1590, doi:10.3390/en16041590.
12. Stephan Bernhard Karmann. Entwicklung eines kompakten volloptischen Zugangs für Großmotoren und Anwendung für die Verbrennungsdiagnostik erneuerbarer Kraftstoffe; Technische Universität München, München, 2023.
13. Eicheldinger, S.; Karmann, S.; Prager, M.; Wachtmeister, G. Optical screening investigations of backfire in a large bore medium speed hydrogen engine. *International Journal of Engine Research* **2022**, *23*, 893–906, doi:10.1177/14680874211053171.
14. Richards, K.J.; Senecal, P.K.; Pomraning, E. *Converge 3.1 Manual*, Madison, WI, 2024. Available online: https://hub.convergecfd.com/downloads/category/2-documentation# (accessed on 12 January 2025).
15. Laget, O.; Malbec, L.-M.; Kashdan, J.; Dronniou, N.; Boissard, R.; Gastaldi, P. Experimental and Numerical Investigations on the Mechanisms Leading to the Accumulation of Particulate Matter in Lubricant Oil. *SAE International Journal of Engines* **2016**, *9*, 2030–2043.
16. Laget, O.; Rouleau, L.; Cordier, M.; Duffour, F.; Maio, G.; Giuffrida, V.; Kumar, R.; Nowak, L. A comprehensive study for the identification of the requirements for an optimal H2 combustion engine. *International Journal of Engine Research* **2023**, doi:10.1177/14680874231167618.
17. Olm, C.; Zsély, I.G.; Pálvölgyi, R.; Varga, T.; Nagy, T.; Curran, H.J.; Turányi, T. Comparison of the performance of several recent hydrogen combustion mechanisms. *Combustion and Flame* **2014**, *161*, 2219–2234, doi:10.1016/j.combustflame.2014.03.006.
18. Frankl, S.; Gleis, S.; Wachtmeister, G. Interpretation of Ignition and Combustion in a Full-Optical High-Pressure-Dual-Fuel (HPDF)

Engine using 3D-CFD Methods. In . CIMAC CONGRESS 19, 29th CIMAC World Congress on Combustion Engine, Meeting the Future of Combustion Engines, Vancouver, BC, CA, Jun 10-14, 2019, 2019.

19. Gleis, S.M. Optische Untersuchung eines diffusiven Dual-Fuel Brennverfahrens für Erdgas sowie alternative Kraftstoffe mit niedriger Zündwilligkeit; Technische Universität München, München, 2022.
20. Dominik Waligorski. Entwicklung eines Druckverlaufsanalyse-Modells auf MATLAB-Basis für einen optisch zugänglichen Großmotor. Wissenschaftliche Arbeit zur Erlangung des Grades M. Sc.; Technische Universität München, München, 2018.
21. Vittorio Rocco. Dynamic T.D.C. and Thermodynamic Loss Angle Measurement in a D. I. Diesel Engine. *SAE Technical Paper Series*.
22. Emiliano Pipitone; Alberto Beccari; Stefano Beccari. The Experimental Validation of a New Thermodynamic Method for TDC Determination. In . 8th International Conference on Engines for Automobiles; Consiglio Nazionale delle Ricerche.
23. Armbruster, F.; Gelner, A.; Zepf, A.; Prager, M.; Härtl, M.; Jaensch, M. Investigations on particle emissions of large-bore engines powered by natural gas and hydrogen. *Environ. Sci.: Adv.* **2024**, doi:10.1039/D4VA00200H.